Supporting Information

Dispersion of Complex Refractive Indices for Intense Vibrational Bands. I Quantitative Spectra

Ryo Murata,[†] Ken-ichi Inoue,[†] Lin Wang,[†,‡] Shen Ye,[*,†,‡] and Akihiro Morita[*,†,‡]

[†]*Department of Chemistry, Graduate School of Science, Tohoku University, Aoba-ku, Sendai 980-8578, Japan*

[‡]*Elements Strategy Initiative for Catalysts and Batteries (ESICB), Kyoto University, Kyoto 615-8520, Japan*

e-mail: ye.shen@tohoku.ac.jp, morita@tohoku.ac.jp

Contents

This Supporting Information presents the detailed data of this work. Sec. S1 provides comprehensive summary of the complex refractive index spectra and analytical formulas for representing the spectra. Sec. S2 presents the non-resonant refractive indices in the infrared region. Secs. S3-S5 deal with possible factors that may affect the accuracy of the present ATR-IR measurement and analysis. Sec. S3 examines the absorption of diamond substrate on the reflectance of ATR measurement. Sec. S4 evaluates the effect of ambient air absorption. Sec. S5 validates our assumption in the ATR analysis about even mixing of *p*- and *s*-polarizations in the incident light source.

S1. Fitting parameters of complex refractive index spectra

This section presents all the complex refractive index spectra of the very strong bands in this work. The complex refractive index of each sample is represented by a set of Lorentz functions in Eq. (S1). The results of optimized Lorentzian parameters of all the bands are also given in the following tables.

$$n_j(\nu) = \eta_j + i\kappa_j = n_j^0 + \sum_{l=1}^{l_{\max}} \frac{A_l}{\nu_l - \nu - i\Gamma_l} \tag{S1}$$

The included parameters in Eq. (S1) are:

- n_j^0= non-resonant refractive index.
- $l_{\max}$ = number of Lorentzian.

- A_l = amplitude of each Lorentzian.
- ν_l = peak frequency of each Lorentzian.
- Γ_l = bandwidth of each Lorentzian.

1. O-H stretch

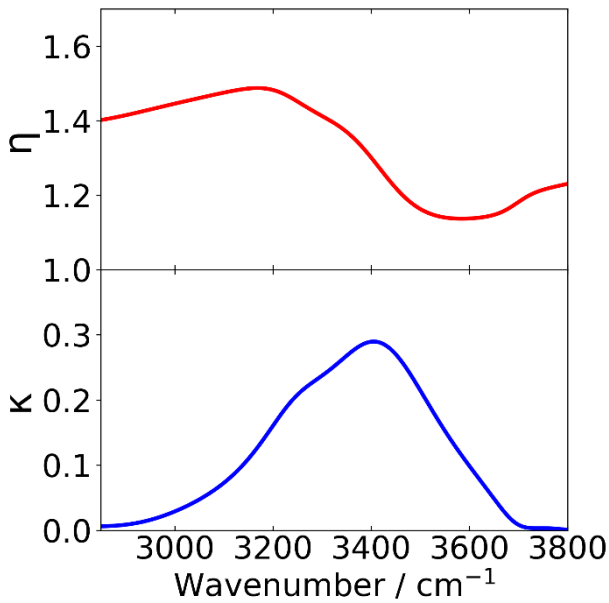

Figure S1. Complex refractive index spectra of liquid water in O-H stretch region. Upper panel: real refractive index $\eta(\nu)$, lower panel: extinction coefficient $\kappa(\nu)$.

Table S1. Optimized Lorentz parameters of water in O-H stretch region

Water in O-H stretch region ($n_j^0 = 1.325,\ l_{\max} = 5$)			
	A_l	ν_l (cm^{-1})	Γ_l (cm^{-1})
1	-3.771	2922	174.7
2	9.111	3244	105.8
3	43.52	3417	158.7
4	-2.775	3696	67.02
5	-5.089	3828	169.2

2. C=O stretch

2-1 Acetone

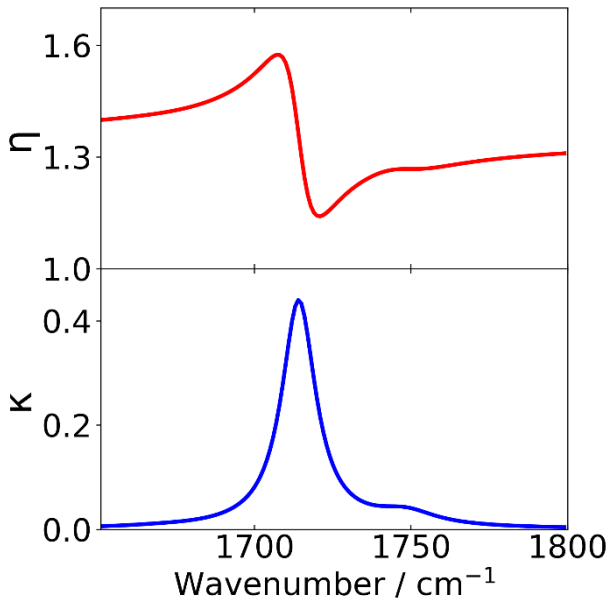

Figure S2. Complex refractive index spectra of liquid acetone in C=O stretch region. Upper panel: real refractive index $\eta(\nu)$, lower panel: extinction coefficient $\kappa(\nu)$.

Table S2. Optimized Lorentz parameters of acetone in C=O stretch region

Acetone in C=O stretch region ($n_j^0 = 1.350,\ l_{\max} = 3$)			
	A_l	ν_l (cm^{-1})	Γ_l (cm^{-1})
1	0.026	1670	14.82
2	2.903	1714	6.641
3	0.317	1748	11.95

2-2 Dimethyl carbonate (DMC)

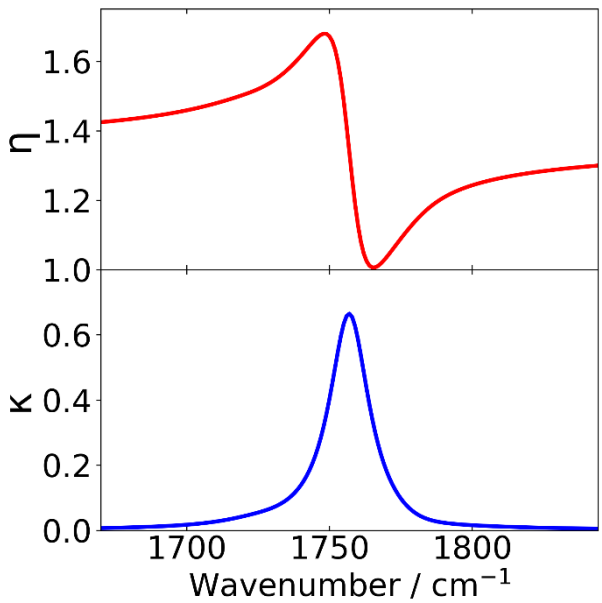

Figure S3. Complex refractive index spectra of liquid DMC in C=O stretch region. Upper panel: real refractive index $\eta(\nu)$, lower panel: extinction coefficient $\kappa(\nu)$.

Table S3. Optimized Lorentz parameters of DMC in C=O stretch region

DMC in C=O stretch region ($n_j^0 = 1.360,\ l_{\max} = 3$)			
	A_l	ν_l (cm^{-1})	Γ_l (cm^{-1})
1	0.173	1724	14.91
2	5.756	1757	8.560
3	-0.446	1779	15.62

2-3 Propylene carbonate (PC)

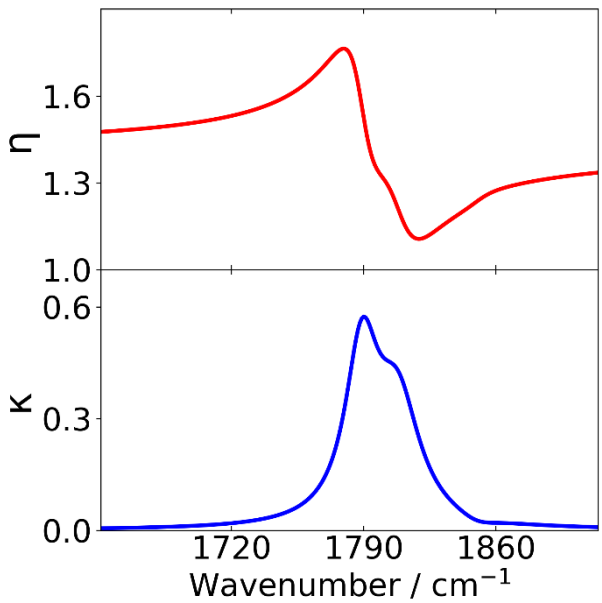

Figure S4. Complex refractive index spectra of liquid PC in C=O stretch region. Upper panel: real refractive index $\eta(\nu)$, lower panel: extinction coefficient $\kappa(\nu)$.

Table S4. Optimized Lorentz parameters of PC in C=O stretch region

PC in C=O stretch region ($n_j^0 = 1.413,\ l_{\max} = 3$)			
	A_l	ν_l (cm^{-1})	Γ_l (cm^{-1})
1	5.189	1790	10.84
2	4.249	1809	13.40
3	-0.259	1852	14.34

2-4 Acetic acid

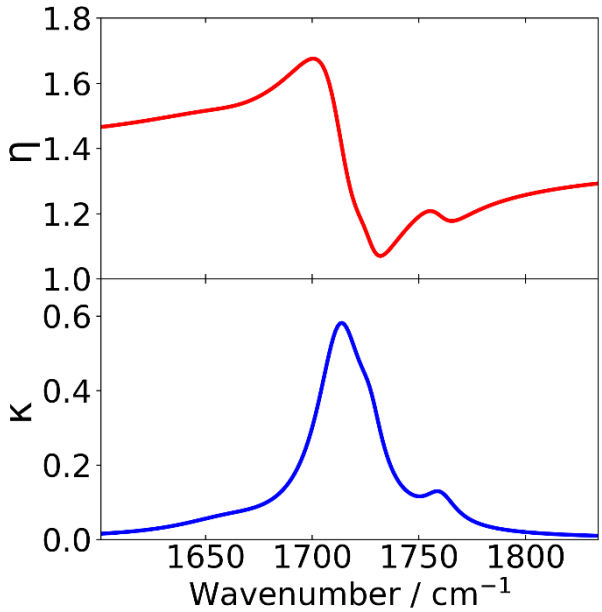

Figure S5. Complex refractive index spectra of liquid acetic acid in C=O stretch region. Upper panel: real refractive index $\eta(\nu)$, lower panel: extinction coefficient $\kappa(\nu)$.

Table S5. Optimized Lorentz parameters of acetic acid in C=O stretch region

Acetic acid in C=O stretch region ($n_j^0 = 1.376,\ l_{\max} = 4$)			
	A_l	ν_l (cm^{-1})	Γ_l (cm^{-1})
1	0.948	1659	28.78
2	7.384	1713	13.61
3	0.946	1727	7.297
4	0.695	1760	9.022

2-5 Acetic anhydride

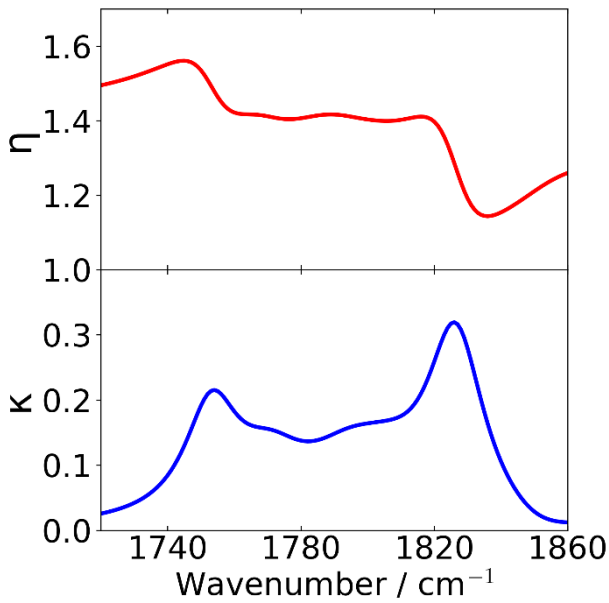

Figure S6. Complex refractive index spectra of liquid acetic anhydride in C=O stretch region. Upper panel: real refractive index $\eta(\nu)$, lower panel: extinction coefficient $\kappa(\nu)$.

Table S6. Optimized Lorentz parameters of acetic anhydride in C=O stretch region

Acetic anhydride in C=O stretch region ($n_j^0 = 1.383,\ l_{\max} = 6$)			
	A_l	ν_l (cm^{-1})	Γ_l (cm^{-1})
1	1.668	1753	9.851
2	0.964	1771	13.13
3	1.258	1794	16.52
4	0.708	1806	15.00
5	3.004	1826	10.42
6	-0.498	1851	15.05

3. C-O stretch

3-1 Methanol

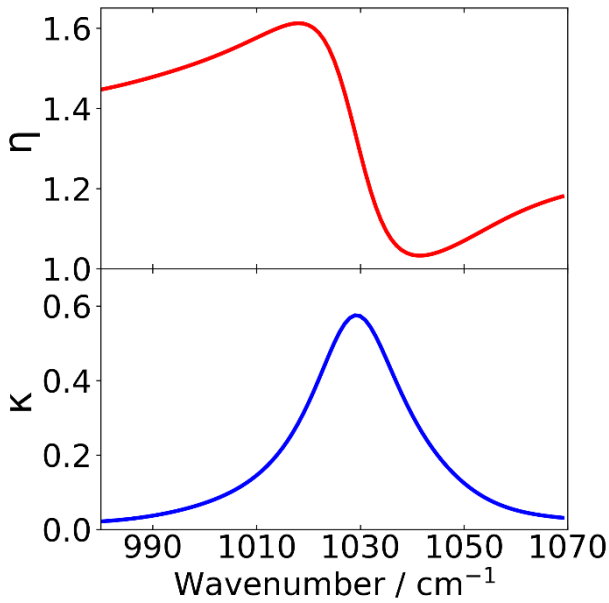

Figure S7. Complex refractive index spectra of liquid methanol in the C-O stretching region. Upper panel: real refractive index $\eta(\nu)$, lower panel: extinction coefficient $\kappa(\nu)$.

Table S7. Optimized Lorentz parameters of methanol in C-O stretch region

Methanol in C-O stretch region ($n_j^0 = 1.325,\ l_{\max} = 4$)			
	A_l	ν_l (cm^{-1})	Γ_l (cm^{-1})
1	-0.205	985.7	19.89
2	5.434	1029	10.65
3	1.822	1036	20.03
4	-0.725	1054	19.38

4. C-C-O asymmetric stretch

4-1 Ethanol

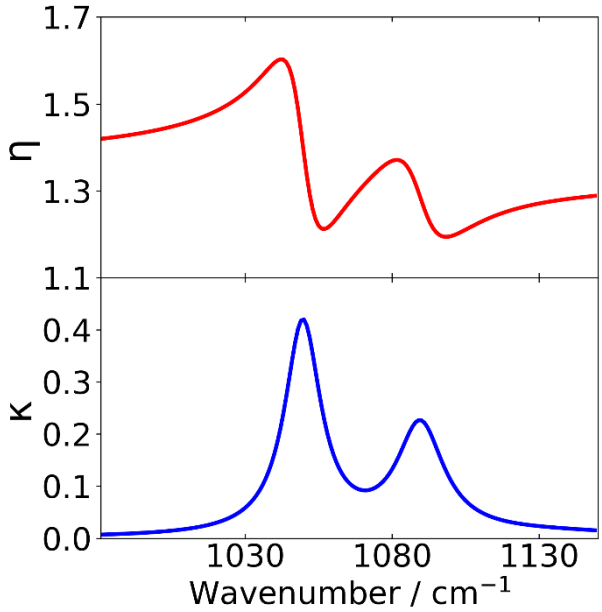

Figure S8. Complex refractive index spectra of liquid ethanol in the C-C-O asymmetric stretching region. Upper panel: real refractive index $\eta(\nu)$, lower panel: extinction coefficient $\kappa(\nu)$.

Table S8. Optimized Lorentz parameters of ethanol in C-C-O asymmetric stretch region.

Ethanol in C-C-O asymmetric Stretch region ($n_j^0 = 1.355,\ l_{\max} = 3$)			
	A_l	ν_l (cm^{-1})	Γ_l (cm^{-1})
1	3.051	1050	7.487
2	2.032	1090	9.709
3	0.346	1135	40.41

4-2 Ethyl acetate (ordinary C-C-O)

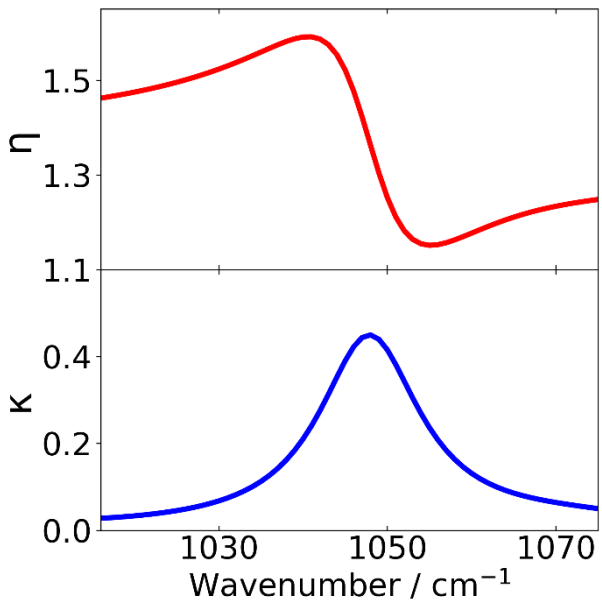

Figure S9. Complex refractive index spectra of liquid ethyl acetate in the ordinary C-C-O asymmetric stretching region. Upper panel: real refractive index $\eta(\nu)$, lower panel: extinction coefficient $\kappa(\nu)$.

Table S9. Optimized Lorentz parameters of ethyl acetate in the ordinary C-C-O asymmetric stretch region.

Ethyl acetate in C-O-C asymmetric stretch region ($n_j^0 = 1.365,\ l_{\max} = 3$)			
	A_l	ν_l (cm^{-1})	Γ_l (cm^{-1})
1	0.132	1000	13.88
2	3.235	1048	7.301
3	0.323	1072	15.73

4-3 Ethyl acetate (carbonyl-included C-C-O)

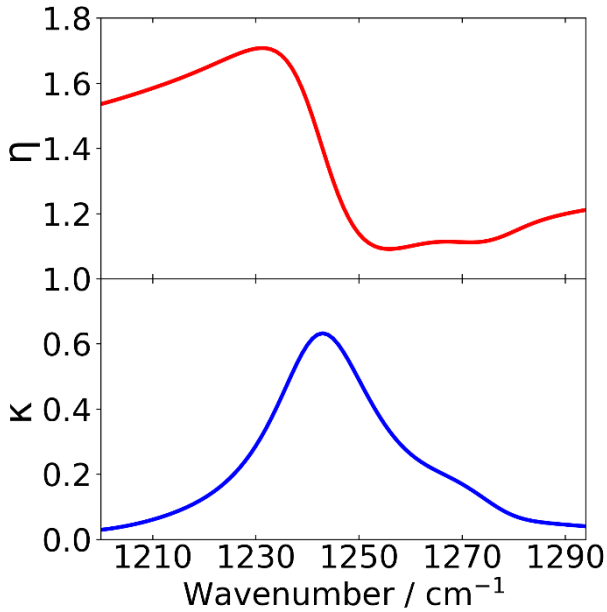

Figure S10. Complex refractive index spectra of liquid ethyl acetate in the carbonyl included C-C-O asymmetric stretching region. Upper panel: real refractive index $\eta(\nu)$, lower panel: extinction coefficient $\kappa(\nu)$.

Table S10. Optimized Lorentz parameters of ethyl acetate in carbonyl-included C-C-O asymmetric stretch region.

Ethyl acetate in C-O-C asymmetric stretch region ($n_j^0 = 1.365,\ l_{\max} = 5$)			
	A_l	ν_l (cm^{-1})	Γ_l (cm^{-1})
1	-0.296	1201	17.81
2	6.665	1242	11.67
3	0.832	1250	11.49
4	1.159	1269	12.63
5	-0.506	1279	13.92

5. C-O-C asymmetric stretch

5-1 Tetrahydrofuran (THF)

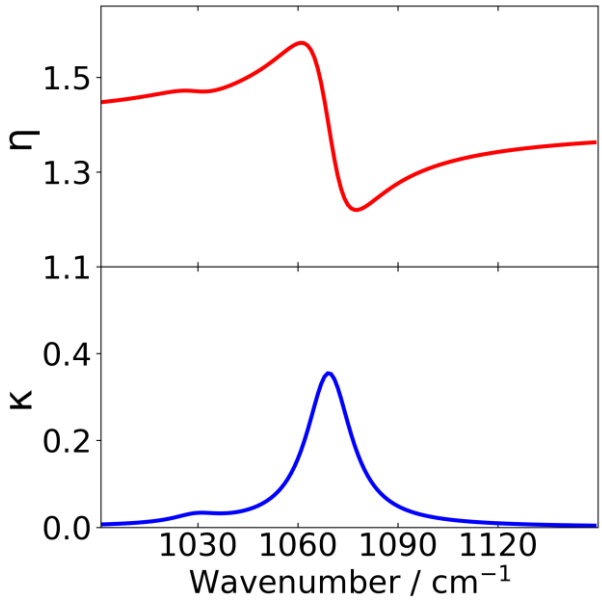

Figure S11. Complex refractive index spectra of liquid THF in the C-O-C asymmetric stretching region. Upper panel: real refractive index $\eta(\nu)$, lower panel: extinction coefficient $\kappa(\nu)$.

Table S11. Optimized Lorentz parameters of THF in C-O-C asymmetric stretch region.

THF in C-O-C asymmetric stretch region ($n_j^0 = 1.400,\ l_{\max} = 2$)			
	A_l	ν_l (cm^{-1})	Γ_l (cm^{-1})
1	0.157	1030	8.527
2	2.920	1069	8.237

5-2 Diglyme

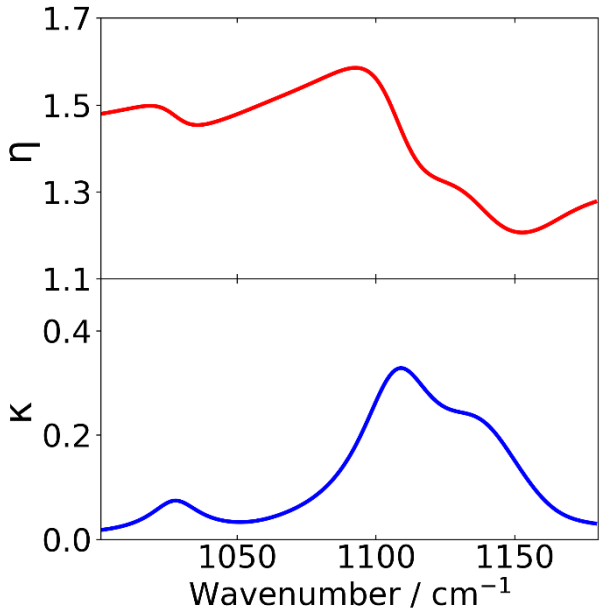

Figure S12. Complex refractive index spectra of liquid diglyme in the C-O-C asymmetric stretching region. Upper panel: real refractive index $\eta(\nu)$, lower panel: extinction coefficient $\kappa(\nu)$.

Table S12. Optimized Lorentz parameters of diglyme in C-O-C asymmetric stretch region.

Diglyme in C-O-C asymmetric stretch region ($n_j^0 = 1.397,\ l_{\max} = 5$)			
	A_l	ν_l (cm^{-1})	Γ_l (cm^{-1})
1	0.659	1028	10.92
2	-0.181	1055	20.21
3	4.525	1108	16.66
4	3.871	1138	21.56
5	-0.722	1164	19.76

5-3 Triglyme

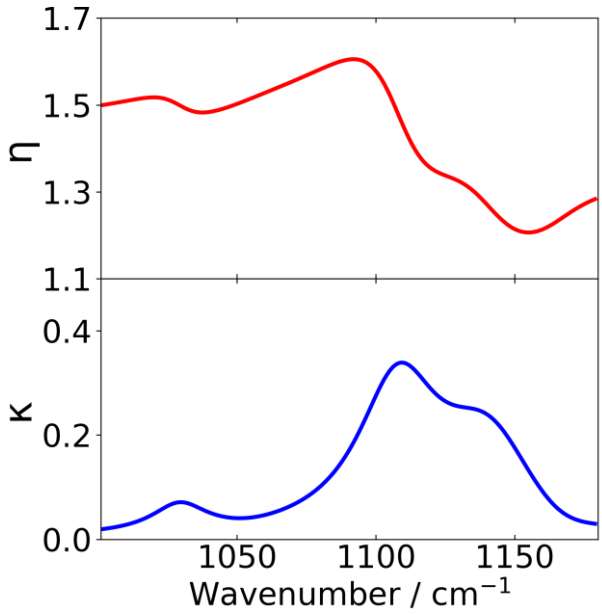

Figure S13. Complex refractive index spectra of liquid trilyme in the C-O-C asymmetric stretching region. Upper panel: real refractive index $\eta(\nu)$, lower panel: extinction coefficient $\kappa(\nu)$.

Table S13. Optimized Lorentz parameters of triglyme in C-O-C asymmetric stretch region.

Triglyme in C-O-C asymmetric stretch region ($n_j^0 = 1.413,\ l_{\max} = 5$)			
	A_l	ν_l (cm^{-1})	Γ_l (cm^{-1})
1	0.667	1029	12.28
2	-0.152	1053	20.43
3	5.004	1108	17.74
4	4.275	1141	22.18
5	-1.014	1166	19.60

5-4 Tetraglyme

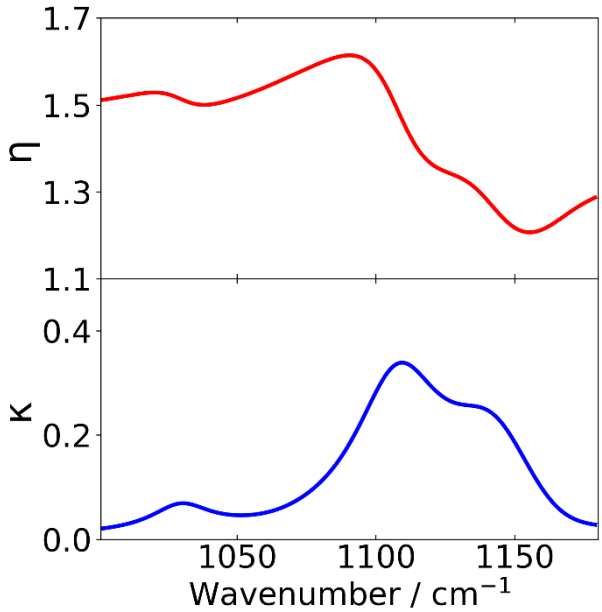

Figure S14. Complex refractive index spectra of liquid tetraglyme in the C-O-C asymmetric stretching region. Upper panel: real refractive index $\eta(\nu)$, lower panel: extinction coefficient $\kappa(\nu)$.

Table S14. Optimized Lorentz parameters of tetraglyme in C-O-C asymmetric stretch region.

Tetraglyme in C-O-C asymmetric stretch region ($n_j^0 = 1.423,\ l_{\max} = 5$)			
	A_l	ν_l (cm^{-1})	Γ_l (cm^{-1})
1	0.649	1030	13.21
2	-0.185	1064	21.94
3	5.589	1108	19.38
4	4.403	1142	21.81
5	-1.406	1165	22.01

6. C-H stretch

6-1 *n*-hexane

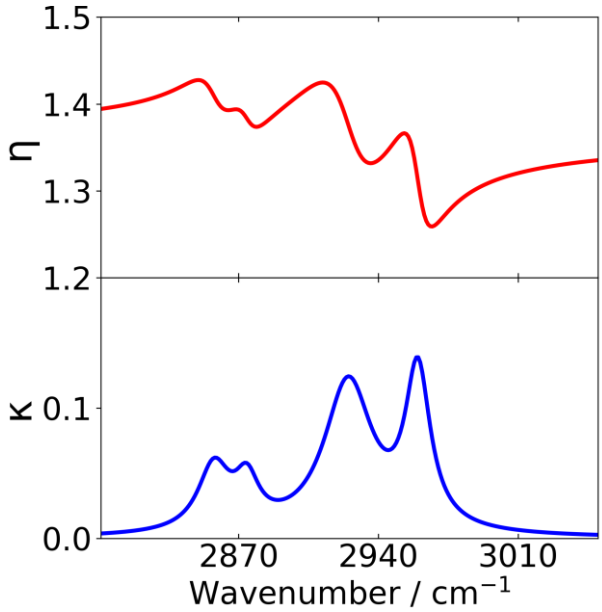

Figure S15. Complex refractive index spectra of liquid *n*-hexane in the C-H stretching region. Upper panel: real refractive index $\eta(\nu)$, lower panel: extinction coefficient $\kappa(\nu)$.

Table S15. Optimized Lorentz parameters of *n*-hexane in C-H stretch region.

n-hexane in C-H stretch region ($n_j^0 = 1.363,\ l_{\max} = 4$)			
	A_l	ν_l (cm^{-1})	Γ_l (cm^{-1})
1	0.481	2858	9.637
2	0.254	2874	7.265
3	1.736	2925	14.82
4	0.917	2960	7.603

6-2 Cyclohexane

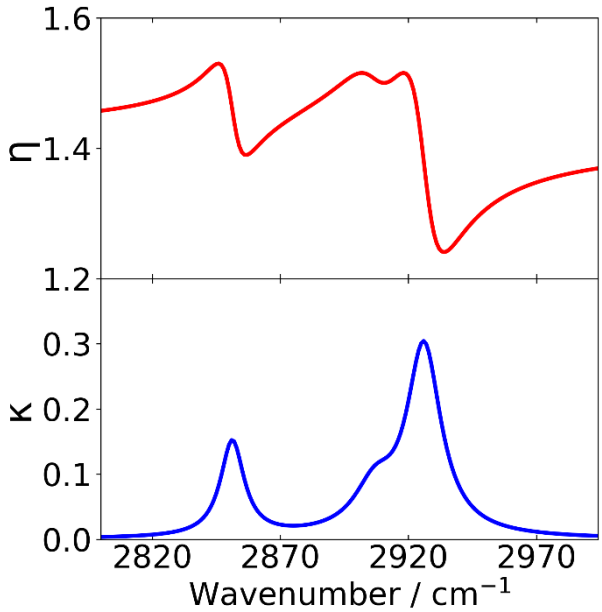

Figure S16. Complex refractive index spectra of liquid cyclohexane in the C-H stretching region. Upper panel: real refractive index $\eta(\nu)$, lower panel: extinction coefficient $\kappa(\nu)$.

Table S16. Optimized Lorentz parameters of cyclohexane in C-H stretch region.

Cyclohexane in C-H stretch region ($n_j^0 = 1.417,\ l_{\max} = 3$)			
	A_l	ν_l (cm^{-1})	Γ_l (cm^{-1})
1	0.826	2851	5.612
2	0.662	2907	9.824
3	2.364	2926	8.166

7. C-H out-of-plane bend

7-1 Toluene

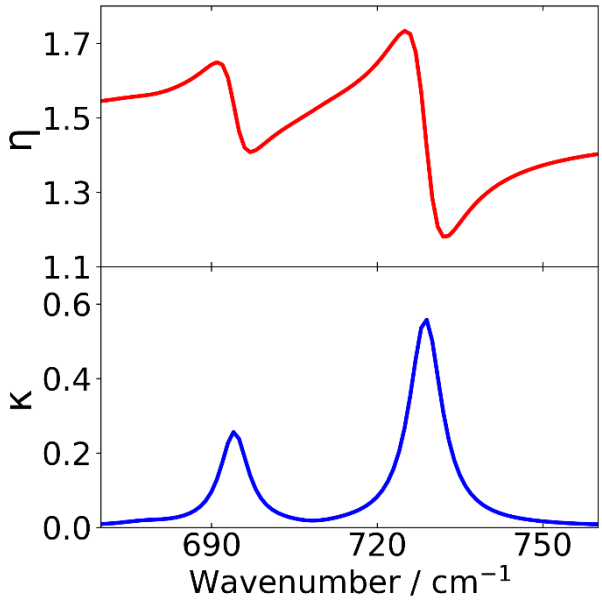

Figure S17. Complex refractive index spectra of liquid toluene in the C-H out-of-plane bending region. Upper panel: real refractive index $\eta(\nu)$, lower panel: extinction coefficient $\kappa(\nu)$.

The minor band at about 680 cm^{-1} is assigned to the C-C bending stretch mode [1], and the major band at 732 cm^{-1} is the C-H out-of-plane bend mode.

Table S17. Optimized Lorentz parameters of toluene in C-H out-of-plane bending region.

Toluene in C-H out of plane bending region ($n_j^0 = 1.477,\ l_{\max} = 4$)			
	A_l	ν_l (cm^{-1})	Γ_l (cm^{-1})
1	0.044	677.7	5.431
2	0.774	694.1	3.084
3	-0.061	708.5	5.923
4	2.006	728.8	3.590

8. NO_2 asymmetric stretch

8-1 Nitrobenzene

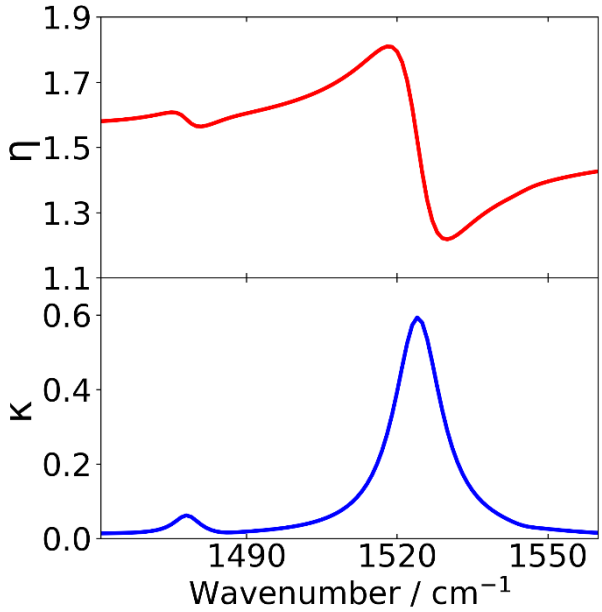

Figure S18. Complex refractive index spectra of liquid nitrobenzene in the NO_2 asymmetric stretching region. Upper panel: real refractive index $\eta(\nu)$, lower panel: extinction coefficient $\kappa(\nu)$.

We notice a side band at 1470 cm^{-1} besides the main band at about 1520 cm^{-1}. The small band is assigned to the C-C stretching vibration "19a" of benzene nucleus [2], and the intense peak at 1520 cm^{-1} is the NO_2 asymmetric stretching mode.

Table S18. Optimized Lorentz parameters of nitrobenzene in NO_2 asymmetric stretch region.

Nitrobenzene in NO_2 asymmetric stretch region ($n_j^0 = 1.520,\ l_{\max} = 5$)			
	A_l	ν_l (cm^{-1})	Γ_l (cm^{-1})
1	0.116	1459	16.81
2	0.169	1478	3.211
3	-0.040	1484	5.103
4	3.411	1524	5.751
5	-0.030	1545	4.012

9. S=O stretch

9-1 Dimethyl sulfoxide (DMSO)

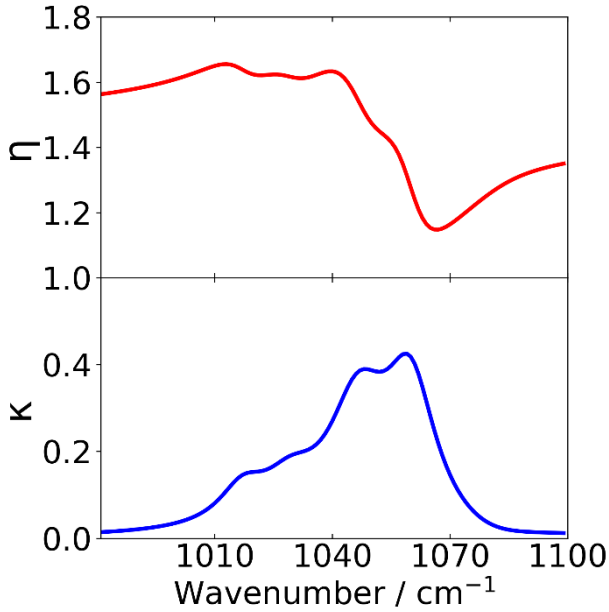

Figure S19. Complex refractive index spectra of liquid DMSO in the S=O stretching region. Upper panel: real refractive index η(ν), lower panel: extinction coefficient κ(ν).

Table S19. Optimized Lorentz parameters of DMSO in S=O stretch region.

DMSO in S=O stretch region ($n_j^0 = 1.465,\ l_{\max} = 5$)			
	A_l	ν_l (cm^{-1})	Γ_l (cm^{-1})
1	0.597	1017	7.311
2	0.759	1029	8.695
3	2.603	1047	9.322
4	2.644	1060	7.992
5	-0.492	1079	14.39

S2. Non-Resonant Refractive Indices

1. Cauchy parameters

The formula of frequency-dependent refractive index in Eq. (S1) includes the non-resonant refractive index n_j^0. The non-resonant refractive index in the infrared region was determined by extrapolating the optical refractive index using the Cauchy's equation [3],

$$n(\lambda) = A + \frac{B}{\lambda^2} + \frac{C}{\lambda^4} \tag{S2}$$

where n is the refractive index, λ is the wavelength in nm unit, and A, B, C are the Cauchy's parameters. These parameters are determined by measuring refractive indices at six different wavelengths in the visible region. Table S20 summarizes the measured refractive indices and the optimized Cauchy's parameters for all the samples.

Table S20. Refractive indices at six wavelengths and the Cauchy's parameters.

Samples	Refractive indices at six wavelengths/nm						Cauchy's Parameters		
	480	486	546	589	644	656	A	B	$C\times10^8$
water	1.338	1.337	1.334	1.332	1.331	1.330	1.324	2072	2.424
acetone	1.363	1.362	1.359	1.357	1.355	1.355	1.350	1302	3.949
DMC	1.373	1.371	1.368	1.367	1.365	1.365	1.360	1144	3.604
PC	1.426	1.425	1.421	1.420	1.418	1.418	1.413	884.3	4.684
acetic acid	1.394	1.393	1.389	1.386	1.384	1.384	1.376	2808	3.167
acetic anhydride	1.395	1.393	1.390	1.388	1.386	1.386	1.383	281.9	5.708
methanol	1.333	1.331	1.329	1.327	1.326	1.326	1.325	-1293	7.107
ethanol	1.366	1.364	1.361	1.360	1.358	1.358	1.355	-216.4	5.769
ethyl acetate	1.377	1.375	1.372	1.370	1.369	1.369	1.365	56.80	5.478
THF	1.413	1.411	1.408	1.406	1.404	1.404	1.400	572.8	5.510
diglyme	1.412	1.411	1.408	1.406	1.404	1.404	1.396	2614	2.091
triglyme	1.428	1.426	1.423	1.421	1.419	1.419	1.412	2149	2.906
tetraglyme	1.438	1.436	1.433	1.431	1.429	1.428	1.422	1837	3.686
n-hexane	1.379	1.378	1.375	1.373	1.371	1.371	1.363	3449	0.575

cyclohexane	1.431	1.429	1.426	1.424	1.422	1.422	1.417	830.2	5.103
toluene	1.508	1.506	1.499	1.495	1.491	1.490	1.476	4798	5.641
nitrobenzene	1.567	1.566	1.553	1.547	1.542	1.541	1.519	7728	7.846
DMSO	1.487	1.485	1.480	1.477	1.475	1.474	1.464	3380	3.998

2. Comparison with Sellmeier's equation

In this work, the non-resonant refractive indices of all samples in the infrared region were determined by the Cauchy's equation (S2). The dispersion relation could be described alternatively using the Sellmeier's equation [4],

$$n^2(\lambda) = 1 + \frac{A\lambda^2}{\lambda^2 - \lambda_0^2} \tag{S3}$$

where n is the refractive index, λ is the wavelength in nm unit, and A, λ_0 are called Sellmeier coefficients. Therefore, we compare the performance of two equations (S2) and (S3) in the case of water as an example. The Sellmeier coefficients of water were determined via the least-square fitting of the refractive indices measured at six different wavelengths (λ = 480 nm, 486 nm, 546 nm, 589 nm, 644 nm, 656 nm) with Eq. (S3). The optimized Sellmeier coefficients were $A = 0.748$ and $\lambda_0 = 110.2$ nm.

Figure S20 shows the dispersion of refractive index using both equations. The extrapolated refractive index at the IR region ($\lambda = 2$ μm or $\tilde{\nu}$=5000 cm^{-1}) is 1.325 and 1.323 by Eq. (S2) and (S3), respectively. The difference of 0.002 is far smaller than the uncertainty in determining the complex refractive indices in the main text.

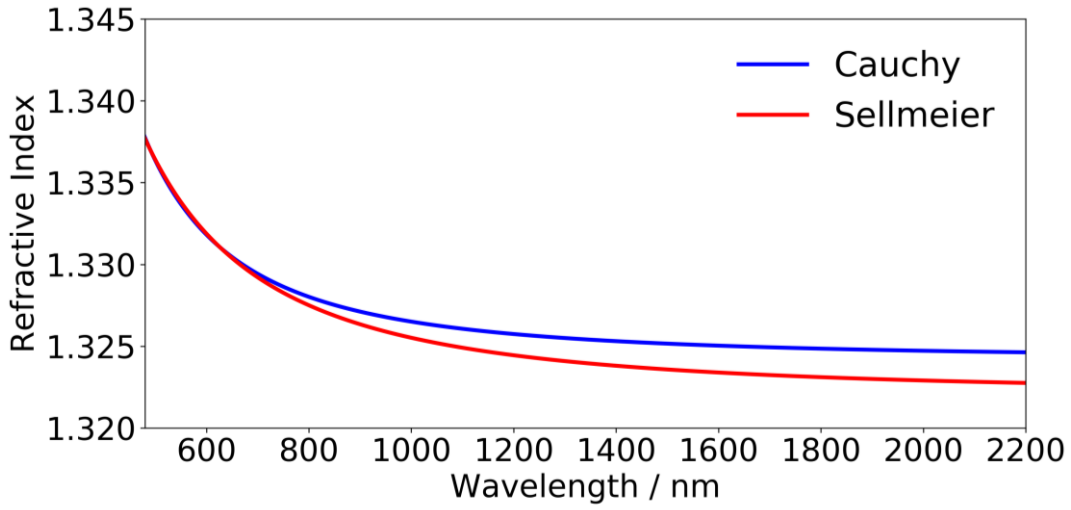

Figure S20. Dispersion of the refractive index of water determined by Cauchy's equation (red line) and Sellmeier's equation (blue line).

S3. Effects on IR absorption

1. Diamond substrate

It is known that diamond has IR absorption in the mid-IR region [5], and thus we examine the possible influence on the present ATR-IR measurement using diamond substrate. The IR absorption of diamond is manifested in Figure S21, which compares the single-beam spectra measured with diamond and ZnSe substrates. ZnSe (n=2.41) is chosen for reference since it has no absorption in the mid IR region and has a comparable refractive index with that of diamond (n=2.38). The apparent difference of the two spectra in Figure S21 shows IR absorption of diamond at around 1700~2700 cm^{-1}. This result suggests that the absorption of diamond substrate may affect the ATR-IR measurement at that region. To evaluate the possible effect, we measured the ATR-IR spectrum of acetonitrile in the C ≡ N stretching region which is overlapped with the diamond absorption band. The C ≡ N band of acetonitrile shows a maximum extinction coefficient about 0.05, which is not regarded as a "very strong" band.

Figure S22 shows the reflectance spectra of acetonitrile measured by using the diamond substrate and ZnSe substrate. The minimum reflectances of the two spectra in the figure differ by 0.5 %. This is within the uncertainty of the ATR measurement. This result indicates that the ATR measurement is insensitive to the absorption of diamond substrate,

arguably because the effective optical path of ATR geometry is very short. The present result has confirmed that the effect of diamond absorption is negligibly small on the ATR results.

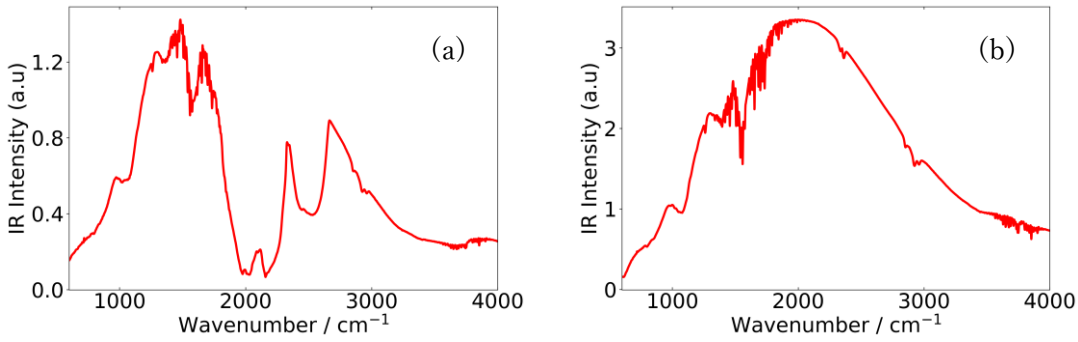

Figure S21. Single-beam spectra with (a) diamond and (b) ZnSe substrates.

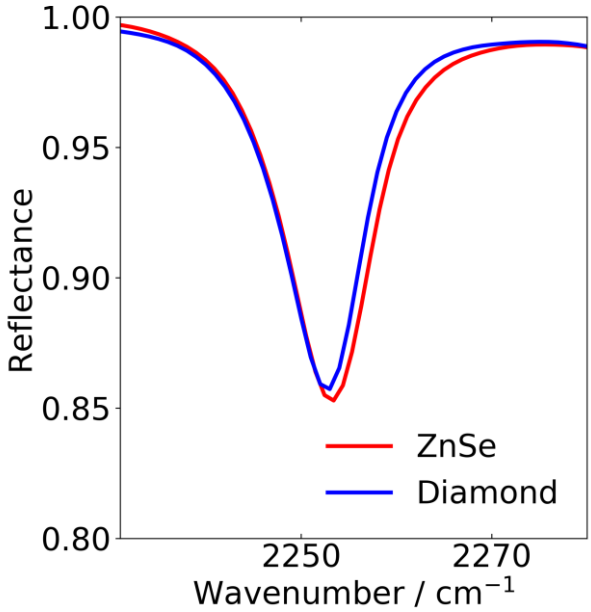

Figure S22. (a) Experimental ATR-IR reflectance spectra of acetonitrile using ZnSe (red line) and diamond (blue line) substrates.

2. Ambient air

The ambient air contains some IR active molecules such as water and carbon dioxide. In particular, water vapor has an absorption band at around 1300~2000 cm^{-1}, which overlaps with the C=O stretching region. Therefore, we examined the possible effect of ambient air absorption in this section. For this purpose, we carried out ATR-IR measurement of acetone in the C=O stretching region after purging the air with nitrogen and compared the result with the spectrum without purging. The difference in the two spectra reveals the effect of ambient air.

Figure S23 shows the ATR-IR spectra with and without purging. The two reflectance spectra were confirmed to agree within 0.8%, which is smaller than the uncertainty of the ATR measurement. This result indicates that the effect of IR absorption of ambient air is negligible in the present ATR measurement.

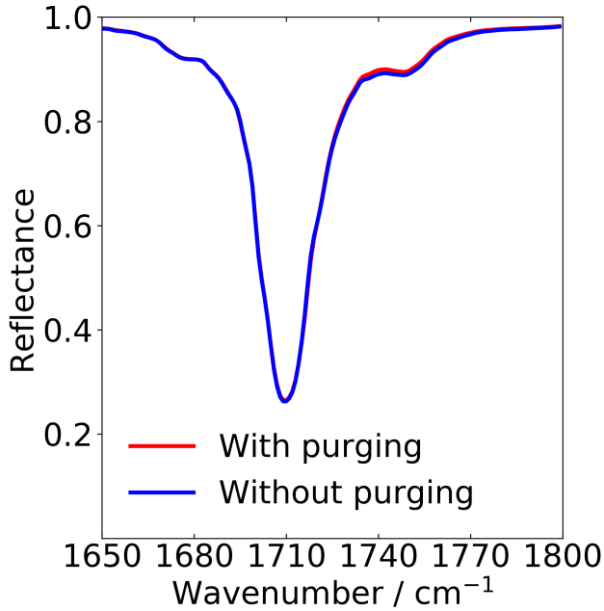

Figure S23. Experimental ATR-IR reflectance spectra of blank air using diamond substrate (Red: with purging. Blue: without purging).

S5. Light polarizations

The present analysis of ATR-IR was performed using unpolarized light sources with the assumption that the *p*- and *s*-polarized components are evenly mixed. Though this assumption appears to be reasonable, we confirm the validity of this assumption here. This assumption in the analysis is represented as

$$\left|r_{ij}^{exp}\right|^2 = \frac{\left|r_{ij}^{p}\right|^2 + \left|r_{ij}^{s}\right|^2}{2} \tag{S4}$$

which indicates that the phenomenological reflectance of unpolarized light, $\left|r_{ij}^{exp}\right|^2$, is the even average of those of *p*- and *s*-polarized light sources. $\left|r_{ij}^{p}\right|^2$ and $\left|r_{ij}^{s}\right|^2$ are the reflectances of *p*- and *s*-polarized lights, respectively, and given in Eqs. (2) and (3) of the main text. To inspect this assumption, we carried out ATR-IR measurements using *p*- and *s*-polarized light sources separately, and compared the results with the result of unpolarized light source with the assumption of Eq. (S4). We chose methanol in the C-O stretching region as an example here.

The ATR-IR reflectance spectra of *p*- and *s*-polarized light sources as well as the unpolarized light are displayed in the left panel of Figure S24. These results show that the reflectance spectra of *p*- and *s*-polarized lights are different, and the that of unpolarized light falls in between. Consequently, we tried to fit the experimental reflectance spectra of *p*- and *s*-polarized lights with the respective formulas of $\left|r_{ij}^{p}\right|^2$ and $\left|r_{ij}^{s}\right|^2$ separately using a common set of Lorentz parameters of complex refractive index. This fitting procedure takes account of different reflectance of *p*- and *s*-polarized lights without the assumption of Eq. (S4). The result of complex refractive index spectra thus derived is compared with that derived from unpolarized light on the basis of Eq. (S4). The right panel of Figure S24 showed that both routes yield quite consistent spectra of complex refractive index, and the discrepancy at the maximum of imaginary spectra is 2 %. This discrepancy is within the uncertainty of the ATR measurement. This result confirms the validity of the assumption of Eq. (S4) in the analysis of ATR spectra using unpolarized light sources.

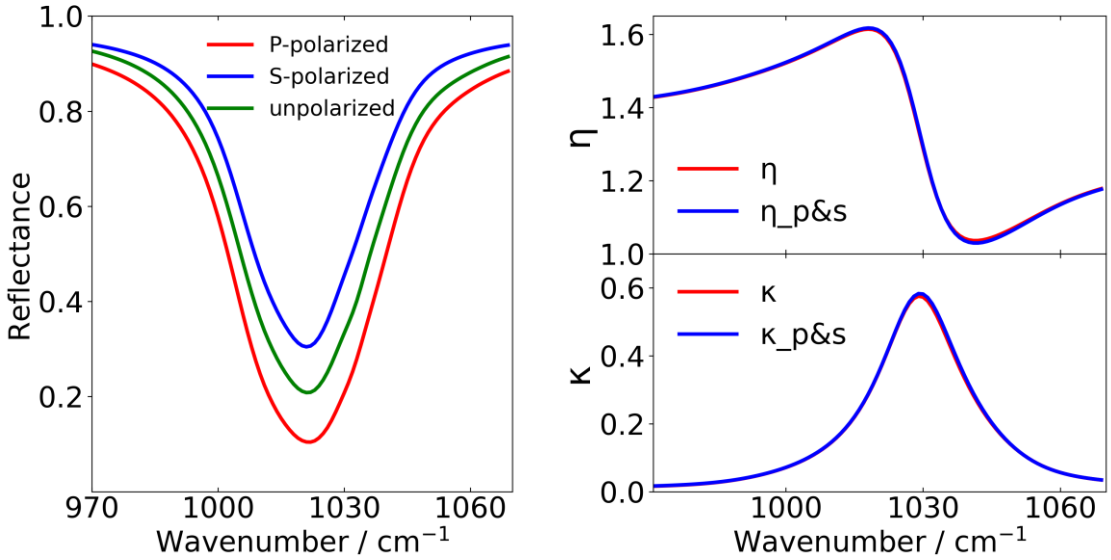

Figure S24. (a) Experimental reflectance spectra in the ATR experiments using diamond. Red: *p*-polarized, blue: *s*-polarized, green: unpolarized. (b) Fitted results of refractive index (η) and extinction coefficient (κ) of methanol in the C-O stretching region. Red: derived from unpolarized light with Eq. (S4), blue: derived from *p*- and *s*-polarized light sources.

References

[1] Smith, B. *Infrared Spectral Interpretation: A Systematic Approach*, CRC Press, Boca Raton, 1999.

[2] Clarkson, J.; Smith, W. E. A DFT analysis of the vibrational spectra of nitrobenzene, *J. Mol. Struct.* **2003**, 655, 413-422.

[3] Jenkins, F. A.; White, H. E. *Fundamentals of Optics*, 4th edition, McGraw-Hill, New York, 1976.

[4] Sellmeier, W. Zur Erklärung der abnormen Farbenfolge im Spectrum einiger Substanzen, *Ann. Phys*. **1871**, *219*, 272–282.

[5] Mildren, R. P. Intrinsic Optical Properties of Diamond. In *Optical Engineering of Diamond*, Mildren, R. P., Rabeau, J., Eds.; Wiley Online Books, 2013; pp 1−34.